Electronic Supplementary Information (ESI)

Cytotoxic sub-nanometer aqueous platinum clusters as potential antitumoral agents

Rossella Greco, Guillermo García–Lainez, Judit Oliver–Meseguer, Carlo Marini, Irene Domínguez, Miguel López–Haro, Juan Carlos Hernández–Garrido, José Pedro Cerón–Carrasco, Inmaculada Andreu* and Antonio Leyva–Pérez*

Table of Contents

Experimental Procedures

General.

Materials. All chemicals were of reagent grade quality, purchased from commercial houses and used without further treatments otherwise indicated. For cell culture experiments, human cervix carcinoma (HeLa), human ovarian cancer (A2780) and cisplatin–resistant (A2780cis) cell lines were purchased from the European Collection of Authenticated Cell Cultures (93021013, 93112519 and 93112517). RPMI-1640 and Dulbecco's modified eagle medium (DMEM)-low glucose (1 g/L) and penicillin–streptomycin solution (1.0 × 105 U/mL, 1.0 × 105 µg/mL) were provided by Invitrogen. Fetal bovine serum (FBS), trypsin-EDTA (0.25–0.02%) and L-glutamine (100 mM) solutions were supplied by Cultek. Phosphate buffered saline buffer (PBS; 0.01 M, pH 7.5), cisplatin (>99% purity), tripan blue solution (0.4 %), Triton-X-100 and 3–[4,5–dimethylthiazole–2–yl]–2,5–diphenyltetrazolium bromide (MTT) were purchased from Merck (Sigma–Aldrich). Dimethyl sulfoxide was supplied by Fagron. Annexin V-FITC apoptosis detection kit was ordered from R&D Systems. Apo-ONE® homogeneous caspase-3/7 assay and Cytotox–ONE homogeneous membrane integrity assay kits were obtained from Promega.

Physical Techniques. The metal content of the samples was determined by inductively coupled plasma–atomic emission spectroscopy (ICP–AES). Solids were disaggregated in aqua regia and later diluted before analysis. ^{1}H, ^{13}C and DEPT NMR spectra were recorded at room temperature on a Bruker AC 300 (300.1 MHz) spectrometer. FT–IR spectra were recorded on a Perkin-Elmer 882 spectrophotometer as KBr pellets. Thermogravimetric analyses were performed on crystalline samples under a dry N_2 atmosphere with a Mettler Toledo TGA/STDA 851^{e} thermobalance operating at a heating rate of 10 ºC min^{-1}. Absorption spectra were recorded on an UV/Vis spectrophotometer (UV0811M209, Varian). Preliminary Scanning Electron Microscopy coupled with Energy Dispersive X–ray (SEM/EDX) was carried out with a XL 30 ESEM (PHILIPS) microscope equipped with a home–made EDX energy dispersive X–ray detector. Fluorescence emission spectra were obtained with a LP S-220B (Photon Technology International) equipped with 75 W Xe lamp. In both cases the MCs where dissolved in water or in a solution of 1-propanol/water (*v/v*, 1:1). X-ray absorption spectroscopy (XAS) measurements were carried out on CLAESS beamline at ALBA Synchrotron Light Source, Barcelona (Spain). Together with the samples, several standard references ($Pt(acac)_2$, PtO_2) have been finely powdered, uniformly mixed with cellulose, and pressed in pellets to ensure the correct absorption jump in transmission. Data reduction has been done using the Demeter program suit: raw data has been normalized by subtracting and dividing pre-edge and post-edge backgrounds as low order polynomial smooth curves. By assuming a linear dependency between the “white line” intensity (taken at the zero of the derivative spectra) and the corresponding electron valence (known for the set of reference compounds), we estimated the oxidation state of the sample. The local structure of the sample has been than refined using the EXAFS signal in the k range 3:12 $Å^{-1}$. Theoretical models for further data analysis have been obtained from platinum and platinum oxide NPs structure using the FEFF6 code and fitted to the EXAFS spectra by adjusting the structural parameters (i.e. coordination number, distances, disorder factors). XPS analyses were performed using a monochromatic

Mg Kα source of 1,253.6 eV, operating at 200 W and $1x10^{-6}$ Pa (ESCA-3400, Shimadzu). The scan step was 0.05 eV. The pass energy was set at 150 eV and a Shirley baseline was removed from all reported spectra. The binding energies were corrected by referencing the C 1s line at 284.8 eV.

Synthesis of metal clusters.

Pt clusters in water (representative procedure): 1.3 g of EVOH29 was initially dissolved in 10 mL of a 1:1 (v:v) 1–propanol:distilled water mixture that was heated at 65 °C under reflux. Once the copolymer was completely dissolved, the mixture was left to cool down at room temperature, after this K_2PtCl_4 was added in order to obtain the metal loadings of 100 nM, 700 nM or 1 μM. These solutions were then stirred overnight. Then, 10 ml of water were added and stirred for 30 min to separate the polymer from the solutions of MCs.
Pt clusters in EVOH films (representative procedure): 13 g of EVOH29 was initially dissolved in 100 mL of a 1:1 (v:v) 1–propanol:distilled water mixture that was heated at 75 °C under reflux. Once the copolymer was completely dissolved, the mixture was left to cool down at room temperature, and after this, K_2PtCl_4 or H_2PtCl_4 was added in order to obtain a metal loading of 0.02 mmol $Pt \cdot g^{-1}$ dry polymer. The resultant suspension was spread on a Teflon–coated glass plate using a 200 μm spiral bar coater. A digital Mitutoyo micrometer was used to determine film thickness, with an average value of 0.012 ± 0.003 mm. The Pt clusters can be released in water by soaking 150 mg of Pt@EVOH in 10 ml of H_2O:EtOH (1:1) for 2 h under stirring and then separating the polymeric matrix. The solution was then kept at -18 °C.

Flow injection–high resolution mass spectrometry
The flow injection–HRMS consisted of an injection and pump systems from Thermo Scientific and a single mass spectrometer Orbitrap Thermo Fisher Scientific (Exactive™) using an electrospray interface (ESI) (HESI–II, Thermo Fisher Scientific) in positive or negative mode. The injector was directly connected to the source and 10 μL of the sample was injected into the flow–injection solvent consisting of an aqueous solution of 0.1% formic acid and methanol (1:1). The flow rate remained at 0.20 ml min^{-1} over 5 min. The ESI parameters were as follows: spray voltage, 4 kV; sheath gas (N_2, >95%), 35 (non–dimensional); auxiliary gas (N_2, >95%), 10 (non–dimensional); skimmer voltage, 18 V; capillary voltage, 35 V; tube lens voltage, 95 V; heater temperature, 305 °C; capillary temperature, 300°C. The mass spectra were acquired employing two alternating acquisition functions: (1) full MS, ESI+, without fragmentation (higher collisional dissociation (HCD) collision cell was switched off), mass resolving power = 25 000 FWHM (full width at half maximum); scan time = 0.25 s; (2) all–ion fragmentation (AIF), ESI+, with fragmentation (HCD on, collision energy = 30 eV), and mass resolving power = 10 000 FWHM; scan time = 0.10 s. The mass range was 150.0–1500.0 *m/z*. The chromatograms were processed using Xcalibur™ version 2.2, with Qualbrowser (Thermo Fisher Scientific).

Advanced electron microscopy characterization

Aqueous clusters. Samples for electron microscopy studies were prepared by depositing one drop of the synthesized clusters solution onto holey–carbon coated Cu grids. After their preparation, the TEM samples were conserved under vacuum conditions. Scanning–Transmission Electron Microscopy studies, using High–Angle Annular Dark–Field, HAADF– STEM, which contrasts are related to the roughly Z^2 atomic number of the elements under the beam, were performed on a FEI Titan Themis 60–300 Double Aberration Corrected microscope operated at 300 kV. We corrected the aberrations of the condenser lenses up to fourth–order, using the Zemlin tableau to obtain a sub–Angstrom electron probe. A condenser aperture of 50 μm yielding an electron probe with a convergence angle of 20 mrad was used. To limit the damage by the electron beam, a fast image– recording protocol was used by combining a beam current of 25 pA, a 2.5 μs dwell time and an automated fine–tuning alignment of A1 and C1 using the OptiSTEM software. To obtain images with good quality, the beam current and image acquisition time were optimized according to the stability of the sample under the beam.
Aimed to quantitatively characterize the Pt clusters, a specific methodology for the digital analysis of the experimental images was developed and coded in a home–made MATLAB script. First, to improve the signal–to–noise, the AC HAADF–STEM images were denoised by combining the Anscombe variance stabilization transform (Anscombe VST) with the Undecimated Wavelet Transform. (UWT). The background from the denoised images were subtracted by disk top–hat filtering, allowing us to improve the visibility of the ultrasmall clusters.
To determine in a fully automated, user–independent and statistically meaningful way the size of the clusters observed in the experimental images, a segmentation based on *k*–means clustering techniques was performed. The segmentation of the clustered images using this threshold resulted in binary images of Clusters Map, where the red objects correspond to the Pt clusters and the blue area to the background. At this point, the size of the clusters can be estimated as the diameter of the circle whose area equals that of the segmented particle (equivalent circle diameter). A total of ≈ 100 clusters were automatically detected after clustering and segmentation.

X–ray absorption spectroscopy.
X–ray absorption spectroscopy (XAS) measurements were carried out on CLAESS beamline at ALBA Synchrotron Light Source, Barcelona (Spain). The XAS data were obtained in fluorescence mode at the Pt L_3-edge (11.564 keV) placing the samples at 45 deg geometry (with respect the incoming beam) by means of a 6 elements Silicon Drift detector from Quantum Detector. Each sample was acquired by 20 scans averaged. Quick–XANES mode was essential in order to closely relate the oxidation state with the cytotoxicity activity. The XAS data were processed using Athena software[S1] for background removal, post–edge normalization, and XANES analysis. The oxidation states of the samples were determined by comparing the measured spectrum to a linear combination of the reference metal foil and the metal complexes spectra. The synchrotron light coming from the multipole wiggler has been first vertically collimated, then monochromatized using two pairs of liquid nitrogen cooled Si(311) crystals and finally focused on the sample position

down to ~500 × 500 μm^2. Rh stripe coating on the two optical mirrors guarantees the higher harmonics rejection. A 4 μm-thick Pt foil (Goodfellow, 99.99%), placed between the transmission and reference ion chambers, has been used for calibrating the energy scale, checking the alignment of scans, and determining the passive electron reduction factor in following data post-processing. Theoretical models for the data analysis were calculated for platinum and platinum oxide (based on the crystal structure of Pt NPs using the FEFF6 code and fitted to the EXAFS spectra with the Artemis software. First shell fitting was performed in r–space after Fourier transformation of the k3–weighted data. The samples were measured using directly the platinum clusters and nanoparticles embedded in the EVOH films. The standard samples were finely powdered, mixed uniformly with cellulose, and pressed in pellets to ensure the Pt L_3–edge X–ray absorption jump close to 1. The synchrotron light coming from the multipole wiggler has been first vertically collimated, then monochromatized using two pairs of liquid nitrogen cooled Si(311) crystals and finally focused on the sample position down to ~500 × 500 μm^2. Rh stripe coating on the two optical mirrors guarantees the higher harmonics rejection. The pellets were mounted in a plastic holder, and the spectra were recorded in fluorescence mode at room temperature by means of a 6 channel Silicon drift detector from Quantum Detectors To avoid radiation damage on the sample, the intensity of incident beam has been carefully filtered. Energy scale has been calibrated by measuring a Pt foil. Several scans were acquired in continuous mode to ensure spectral reproducibility and good signal–to–noise ratio. Standard procedure based on the cubic spline fit to the pre–edge subtracted absorption spectra was used to extract the EXAFS signal to determine local structural parameters.

X–ray photoelectron spectroscopy (XPS).
Samples were prepared by dropping a solid water suspension onto a molybdenum plate followed by air drying, and then measurements were performed on a SPECS spectrometer equipped with a Phoibos 150 MCD–9 analyzer using non–monochromatic Mg KR (1253.6 eV) X–ray source working at 50 W. As an internal reference for the peak positions in the XPS spectra, the C1s peak has been set at 284.8 eV. CasaXPS software was used for the data treatment.

Cell culture experiments.

Cell culture conditions. HeLa, HEK-293 and human fibroblasts cells were grown in DMEM medium supplemented with 10% FBS, 4 mM L-Glutamine, 100 U/mL penicillin and 100 μg/mL streptomycin, whereas A2870 cells were grown in RPMI–1640 medium supplemented with 10% FBS, 4mM L–glutamine, 100 U/mL penicillin and 100 μg/mL streptomycin. In the case of A2870cis cells 1 μM cisplatin was added in order to maintain its resistance. Cells were routinely cultured in exponential growth, splitting ratio 1:10 twice per week, in 75 cm^2 plastic flasks in a humidified incubator (5% CO_2 atmosphere) at 37 ºC. For each experiment viability of the cultures was checked by trypan blue exclusion assay and it was higher than 95%.
Metal cluster cell uptake. HeLa cells were seeded at a density of 1.5 × 10^4 cells/well in 24–well plates. Next day, cultures were treated with 0.5 μM of Pt NC or cisplatin and incubated for 4h. Then, cell supernatants were collected and cells were washed once with PBS and then they were lysed using a 10% Triton–100 solution. All samples were stored at –20ºC until its quantitation by ICP–AES.
For advanced electron microscopy characterization, HeLa cells treated overnight with MC were fixed and washed with distilled water, then dehydrated in increasing ethanol solutions (30%, 50%, 70% and 90%), and afterwards, post–fixated with osmium tetroxide (in different concentrations, 0.25% and 1%) in sucrose. Subsequently, a LR-White resin was infiltrated in increasing concentrations until reaching 100%. Polymerization was carried out in an agar capsule at 60 ºC for 24 hours. Ultrafine cuts were made at 60 nm in a Leica UC7 ultramicrotome, with Diatome diamond blade. Both 300 MESh carbon grids and eyelet grids were used.
Cytotoxicity Assay. Cells were seeded in 96–well plates at a density of 2.5 × 10^3 cells/well for HeLa and HEK cell lines and 1.0 × 10^4 for human fibroblasts, A2870 and A2870cis cell lines. Next, cells were treated with Pt MC at eight concentrations ranging from 0.01 to 3 μM. Cisplatin was used as cytotoxic standard compound (0.1–50 μM). After 24 h of treatment, 3–[4,5–dimethylthiazole–2–yl]–2,5–diphenyltetrazolium bromide (MTT) was added at 0.5 mg/mL and incubated for 4 h at 37 ºC. Finally, medium was removed and the purple MTT–formazan product was solubilized in 100 μL of dimethyl sulfoxide (DMSO). Plates were read at 540 nm using a Synergy H1 multi–mode microplate reader (Biotek). For each compound, dose–response curves were determined, allowing the calculation of IC_{50} values (concentration of compound causing a 50% reduction of the formazan product formation) with the Graph Pad 5.0 software.
Fluorescence microscopic analysis of cell death using Annexin–V/ propidium iodide staining. HeLa cells were seeded at a density of 1.5 × 10^4 cells/well in 24–well plates. Next day, plates were treated with the Pt MC at IC_{50} concentrations (previously determined by the MTT assay) for 24 h. Cells were then incubated with 5 μL annexin V–FITC and 50 μL propidium iodide for 30 min avoided from light (R&D Systems) Finally, cell cultures were imaged with the Leica fluorescence microscope PAULA using contrast phase for cell morphology, green LED filter (λ_{exc}=488nm) for annexin–V staining and the red LED filter (λ_{exc}=543nm) for propidium iodide. Representative images were selected from three different regions of the well–plate.
Caspase–3 activation assay. HeLa cells at 1.0 × 10^4 cells/well seeded in 96–well black plates, were treated with the Pt MC at IC_{50} concentrations for 24 h. Next day, 100 μL of caspase–3 substrate (bis–N–CBZ–L–aspartyl–L–glutamyl–L–valyl–L–aspartic acid amide; Z–DEVD–R110), diluted in Apo–ONE® Homogeneous Caspase–3/7 Buffer (R&D Systems) was added to each well. Fluorescent Rhodamine R110 release was continuously monitored using the Synergy H1 multi–mode microplate reader at 37 ºC (λ_{exc} = 499 nm, λ_{em} = 521 nm).
Lactate dehydrogenase (LDH) release assay. Cells were plated in 96–well plates at a density of 1.0 × 10^4 cells/well. After, cells were treated with the Pt MC at IC_{50} concentrations for 24 h. Next day, cell membrane integrity was evaluated using the Cytotox–ONE Homogeneous Membrane Integrity Assay Kit (Promega) according to the manufacturer instructions. Briefly, 80 μL cell culture supernatants were mixed with 80 μL substrate and incubated at room temperature in dark conditions for 30 min. Fluorescence was recorded (λ_{exc} = 560 nm, λ_{em} = 590 nm) using the Synergy H1 multi–mode microplate reader. As the maximum LDH release control, untreated cells were lysed with 10% Triton. The relative release of LDH was calculated using the subsequent formula:

$$\text{Release of LDH}\ (\%) = 100\ \text{x}\ (\text{Fluorescence treated cells} - \text{Fluorescence untreated cells}) / (\text{Fluorescence maximum release} - \text{Flurescence untreated cells})$$

Nuclear DNA photodamage by comet assay. Single cell gel electrophoresis assay (comet assay) was carried out as previously described (García-Lainez et al., 2021) in order to detect strand breaks and alkaline labile sites on nuclear DNA. Briefly, HeLa or human fibroblasts (1.0×10^5 cells/well) were treated with 0.5 μM Pt MC for 24 h. Next day, cells were trypsinized and resuspended in cold PBS. Then, Then, 100 μL of each sample was homogenized with 100 μL of 1% low melting point agarose solution and mixtures were placed forming drops (2.0×10^4 cell/gel) onto Trevigen® treated slides, allowing their jellification. Next, slides were immediately immersed in a container filled with lysis buffer (2.5 M NaCl, 0.1 M Na_2EDTA, 0.01 M Tris, 1 % Triton X-100) and incubated overnight at 4 ºC. Next day, all slides were transferred to a Trevigen® comet assay electrophoresis tank and covered with cold alkaline buffer (0.2 M NaOH, 1 mM EDTA, pH ≥ 13) and let during 40 min for DNA unwinding at 4 ºC. Afterwards, the electrophoresis was carried out at 21 V (1 V/cm) for 30 min at 4 ºC. Once the electrophoresis finished, the slides were washed twice in PBS for 5 min. DNA was fixed by two subsequent incubations with 70 % ethanol and 100% ethanol solutions. Then, DNA was stained with SYBR Gold® (1:10.000 dilution in TE buffer – Tris-HCl 10 mM pH 7.5, EDTA 1 mM) for 30 min at 4 ºC in darkness. Finally, the slides were air-dried and kept in dark conditions. Comet nucleoids and tails were visualized using a Leica DMI 4000B fluorescence microscope (λ_{exc} 490 nm). At least 100 cells/sample were analyzed to determine DNA damage. The percentage of DNA damage of each sample was calculated with the visual scoring of at least 100 DNA comets using the subsequent formula (Møller, 2006): [(Nclass 0 comets × 0) + (Nclass 1 comets × 1) + (Nclass 2 comets × 2) + (Nclass 3 comets × 3) + [(Nclass 4 comets × 4) + (Nclass 5 comets × 5) + (Nclass 6 comets × 6)]/6, where class 0 comets indicate comets with no DNA damage and class 6 comets indicate comets with maximum DNA damage**.**

***Adduct formation*.** Pt MC (200 nM) was incubated with a guanine solution (1 μM) for 24 h at room temperature. Then, mixtures were analyzed in a 5800 MALDI TOF/TOF (ABSciex) in reflector positive mode from 100 to 2500 m/z, at a laser intensity of 3800 (D14-D16), 5300 and 5800 (D17) or 4600 (C14-C17). In this context, 1μL of each sample was spotted onto the MALDI plate and allowed to air-dry at room temperature. After that, 1μL of a matrix (10mg/mL CHCA (Bruker) in 70% ACN, 0.1% TFA) was spotted onto the same MALDI plate position and allowed to air-dry at room temperature.

Computational methods

A series of MC model systems with 3–10 Pt atoms were initially generated by using as a template the structures recently reported, where the stability of transition metal clusters is a function of their atomicity.[S2,S3] Platinum oxide clusters were based on the reported structures by Mackenzie, Fielicke and co–workers.[S4] The reactivity of MCs with a guanine is next predicted within the density functional theory (DFT) framework. We imposed as the only prerequisite that the reaction takes place at the N7 site of guanine, which is the most reactive atom for DNA platination.[S5,S6] For the records, the geometries were fully optimized at the M06/def2SVP level of theory, used in all atoms, while Pt centres are treated with the same functional but with the effective core potentials def2–ECP to account for scalar relativistic effects.[S7,S8] This same protocol was used to analyse all vibrational modes, which allow us to confirm that calculations reach to true minima in the potential energy surface (absence of imaginary frequencies), or a transition state (one imaginary frequency along with the reaction coordinate). Transition states were confirmed to connect reactants and products by performing intrinsic reaction coordinate (IRC) calculations.[S9] The interaction energies of resulting guanine–MC adducts are finally computed with the counterpoise scheme, that correct the basis set superposition error.[S10] All DFT calculations were conducted as implemented in Gaussian 16.[S11]

Results and Discussion

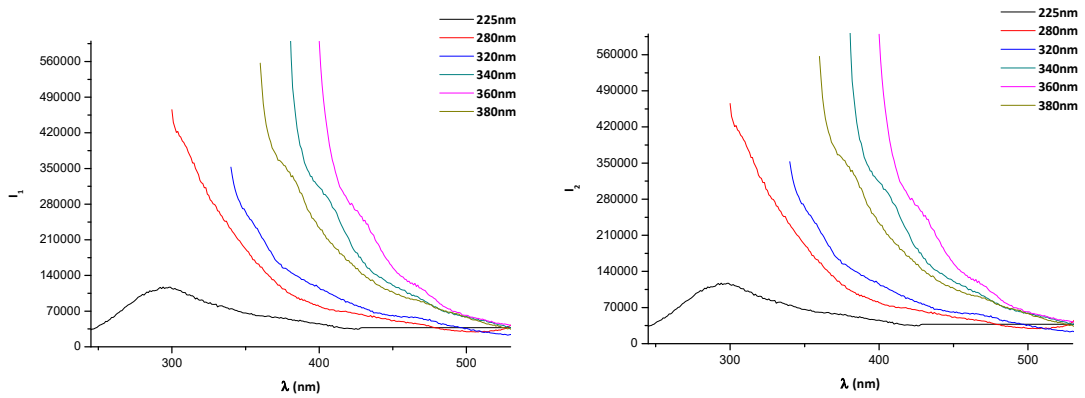

Figure S1. Emission spectra for two different samples of Pt clusters in water/EtOH solution, released from two different films of EVOH and irradiated at increasing wavelenghts (225 to 380 nm). Emission is found at wavelenghts which corresponds to $Pt_{3\text{-}10}$ according to the jellium model: $E_g = E_{Fermi}/N^{1/3}$. N number of atoms in the clusters. E_g emission energy. E_{Fermi} Fermi energy of the bulk material (E_{Fermi} for Platinum is 8.62 eV^2). E_g= 223 nm, N= 3. E_g= 310 nm, N= 10.

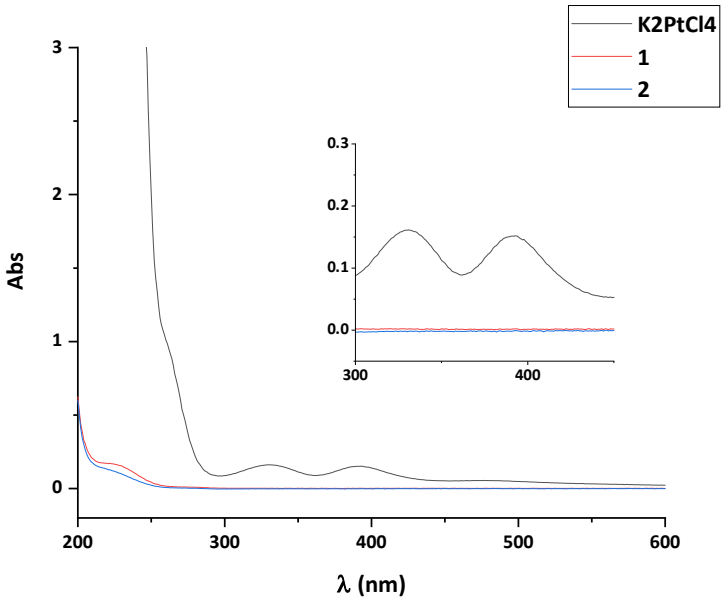

Figure S2. UV-vis adsorption measurements for Pt clusters in water/EtOH solution, released from two different films of EVOH, and K_2PtCl_4. The inset emphasizes the absence of atomic and plasmonic bands from K_2PtCl_2 and Pt NPs.

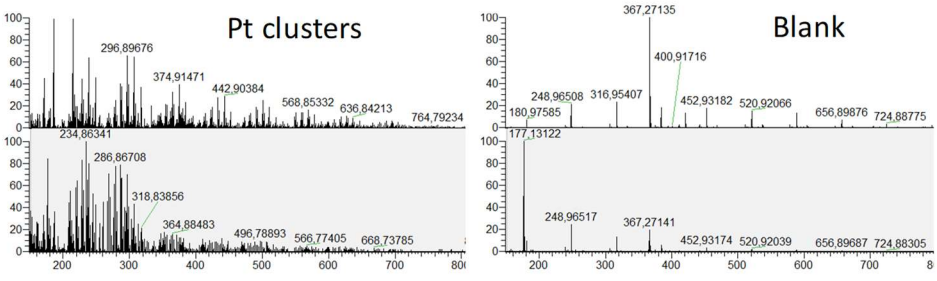

Figure S3. Orbitrap mass chromatogram (negative mode) of Pt clusters in water (left) and water/^{i}PrOH solvent after heating EVOH (blank, right).

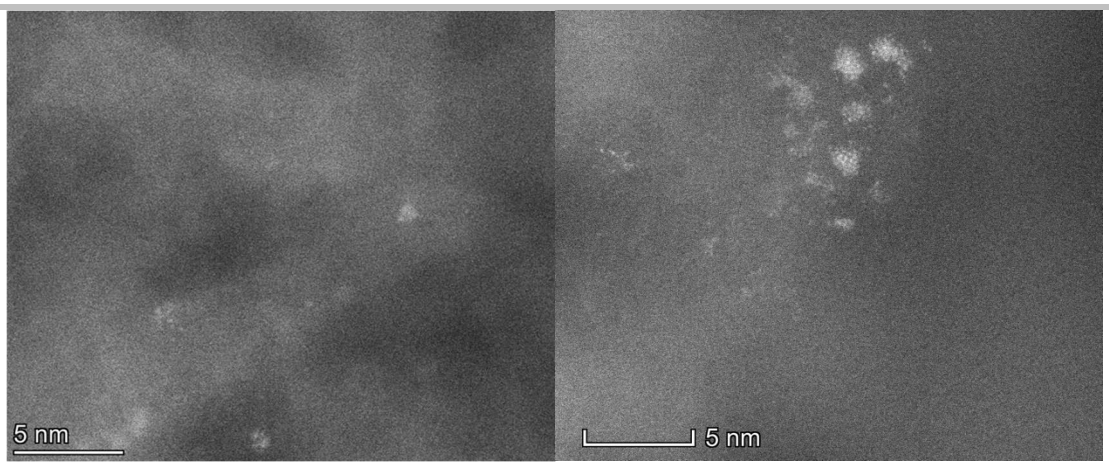

Figure S4. Visualization of Pt species on aqueous solution directly supported onto Cu-carbon grids, performed by means of High-Angle Annular Dark-Field HAADF-STEM images, which contrasts are related to the roughly Z^2 atomic number of the elements under the beam.

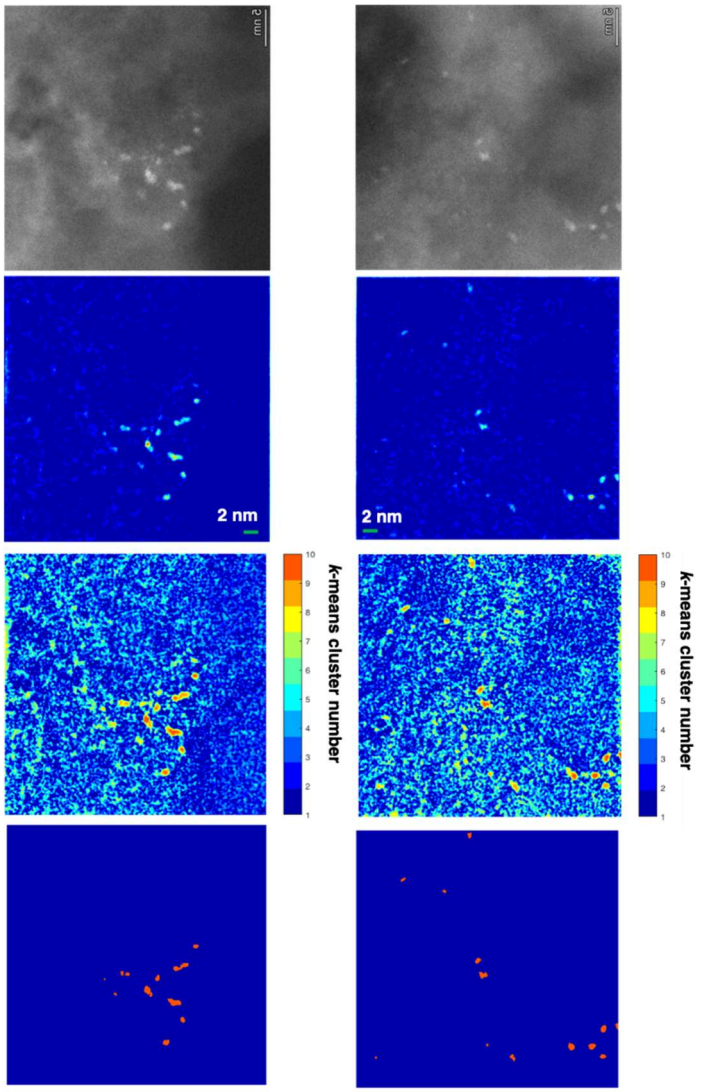

Figure S5. Analysis of AC HAADF-STEM images of Pt cluster aqueous solution by the *k*-means clustering method, resulting from several raw images after denoising and background subtraction. A total number of ≈ 100 clusters have been automatically detected and measured after clustering and segmentation.

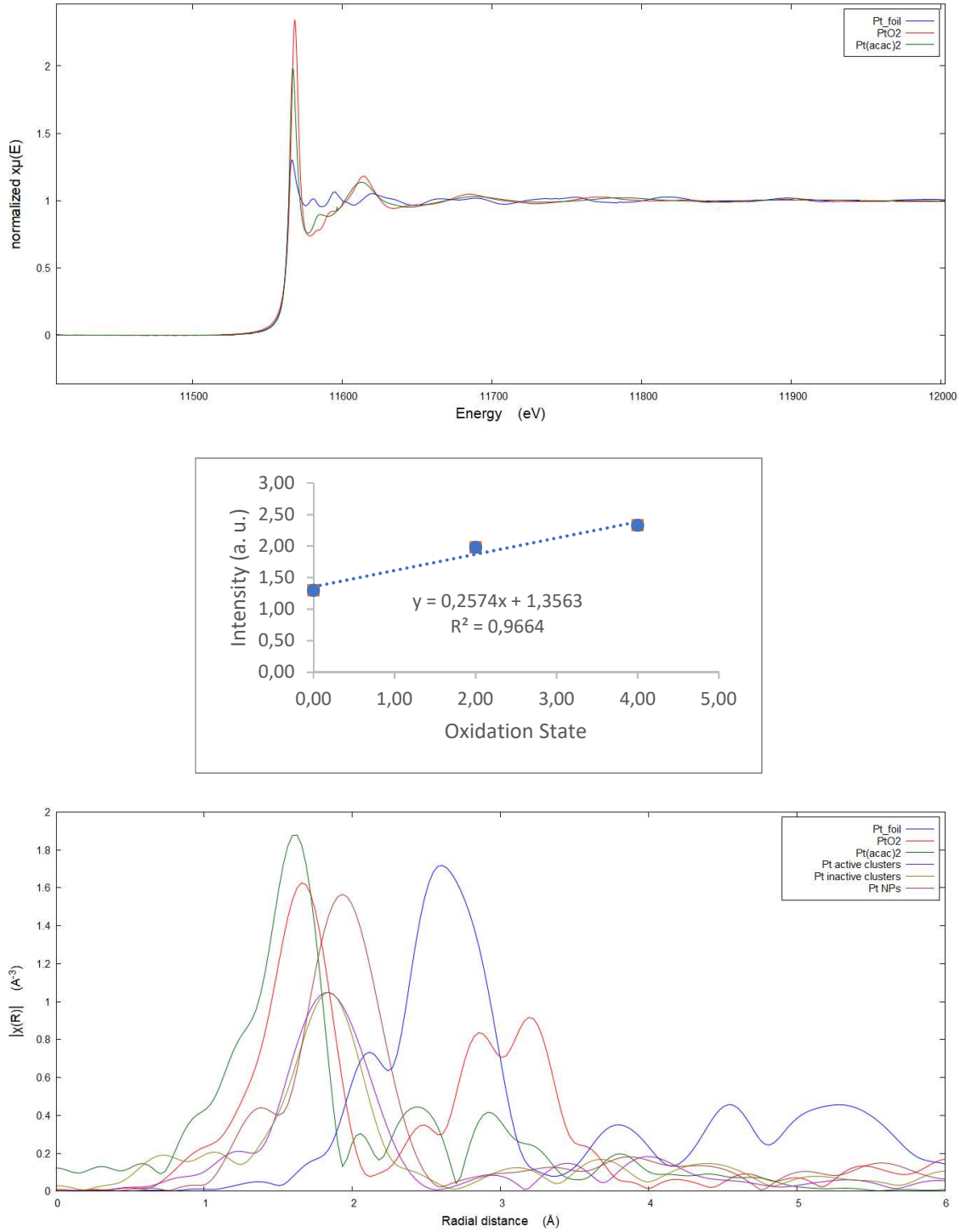

Figure S6. Top) Pt L_3-edge NEXAFS of 3 different Pt@EVOH samples compared with the standard sample. Middle) Calibration curve to obtain the oxidation state, plotting the white line vs. oxidation state. Bottom) EXAFS spectra of the Pt L_3-edge of different the Pt@EVOH samples compared with the standard samples.

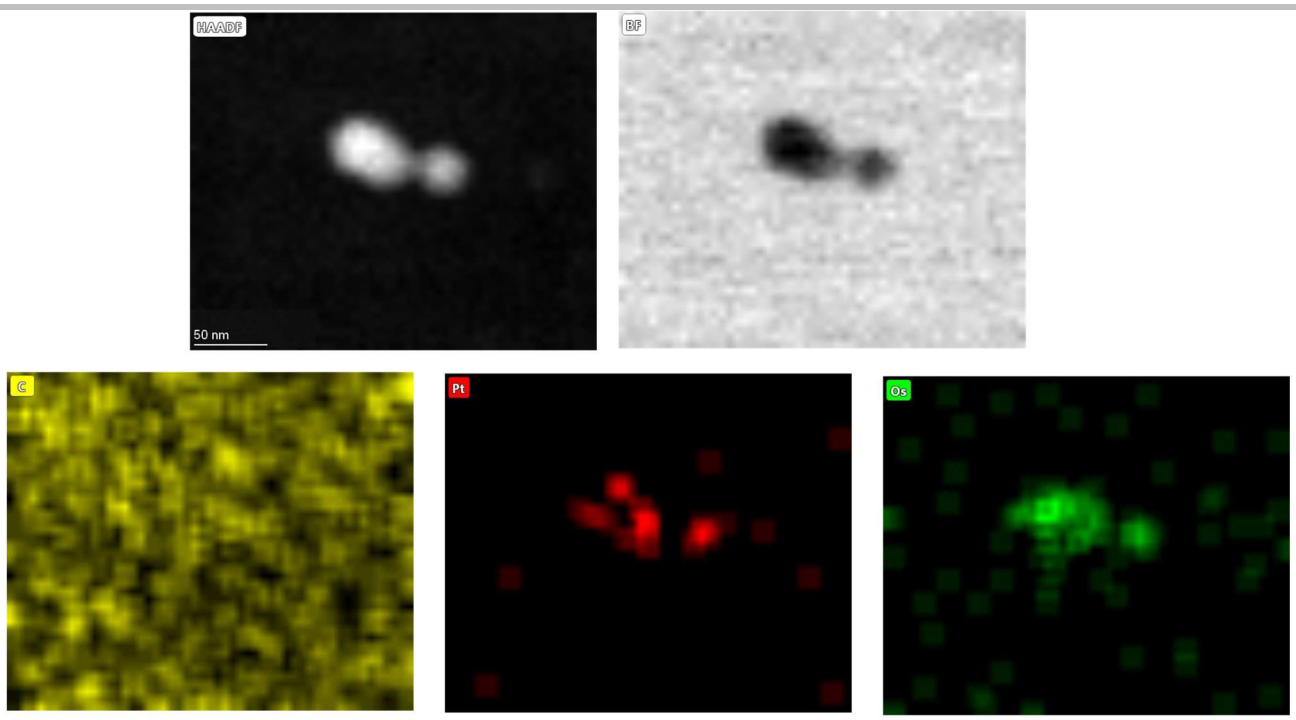

Figure S7. AC–HAADF–STEM images of a HeLa sample treated with Pt MCs, and the corresponding energy-dispersive X-ray spectra of a Pt cluster (bottom).

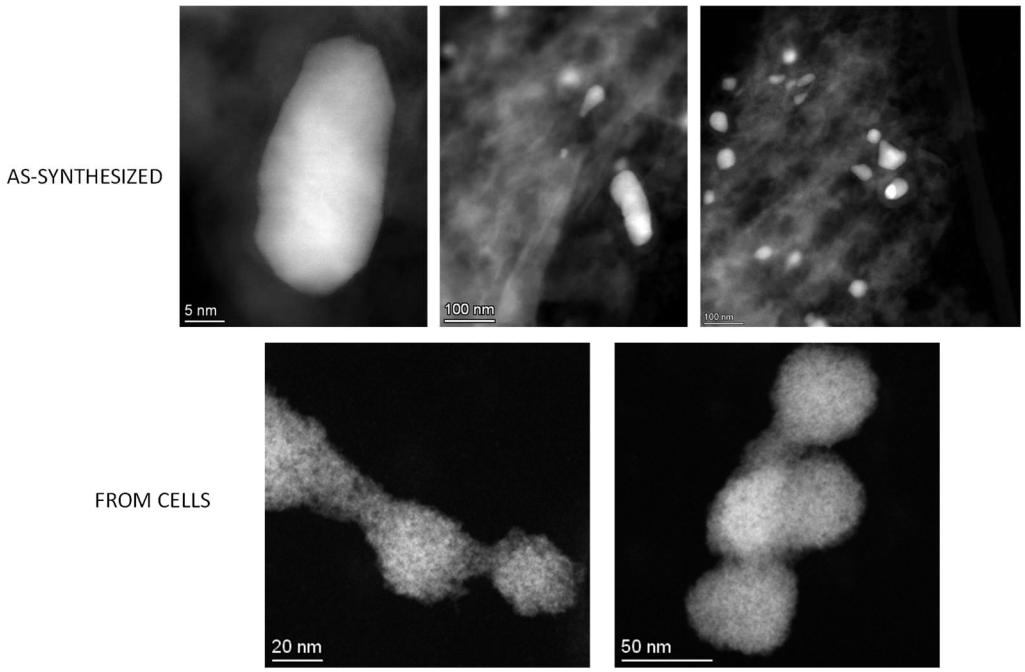

Figure S8. AC–HAADF–STEM images of the residual Pt NPs in the Pt MCs compared to the Pt NPs found within the treated cells.

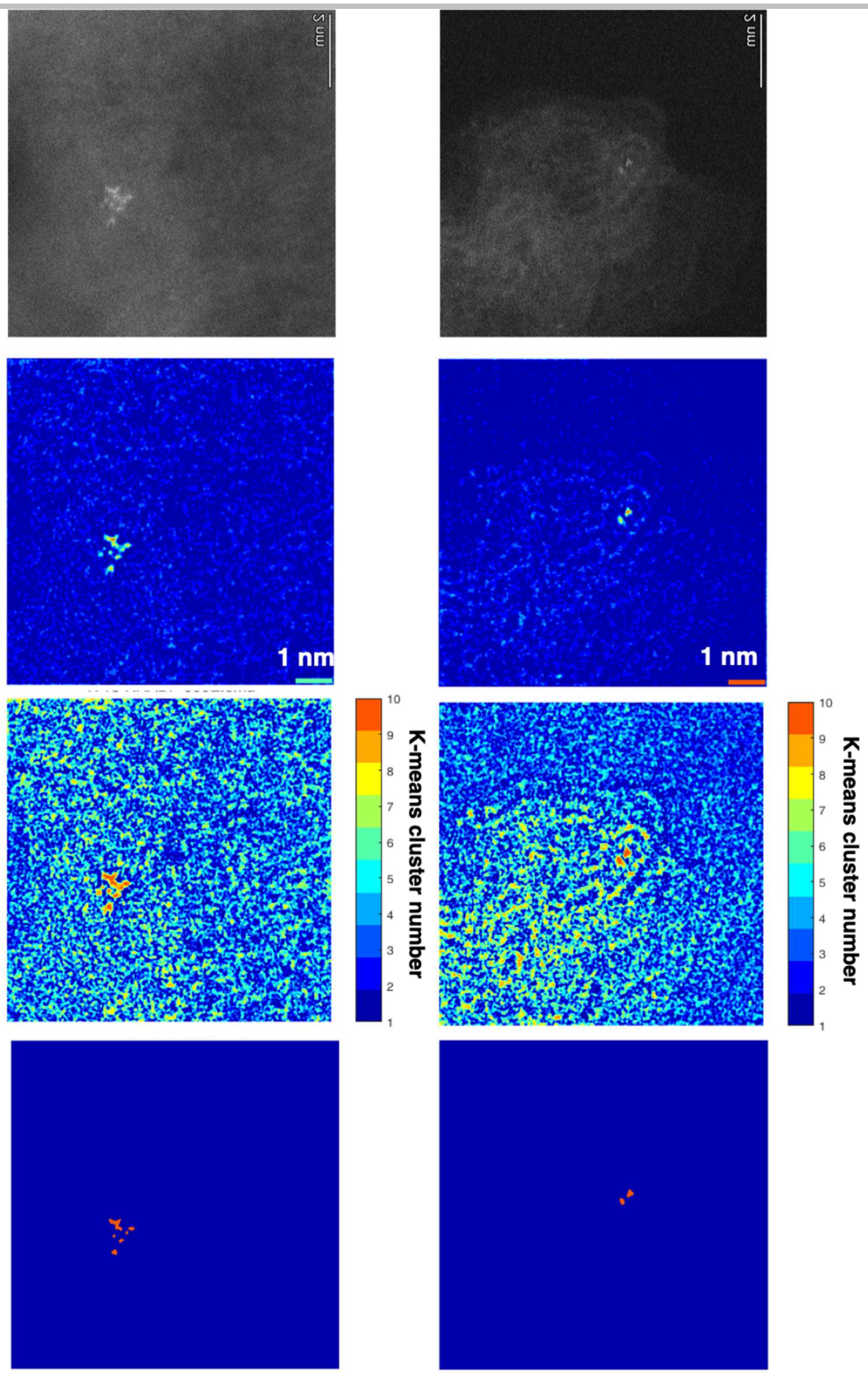

Figure S9. A different second analysis of AC HAADF-STEM images of Pt cluster aqueous solution in charcoal by the *k*-means clustering method, resulting from several raw images after denoising and background subtraction. A total number of ≈ 100 clusters have been automatically detected and measured after clustering and segmentation.

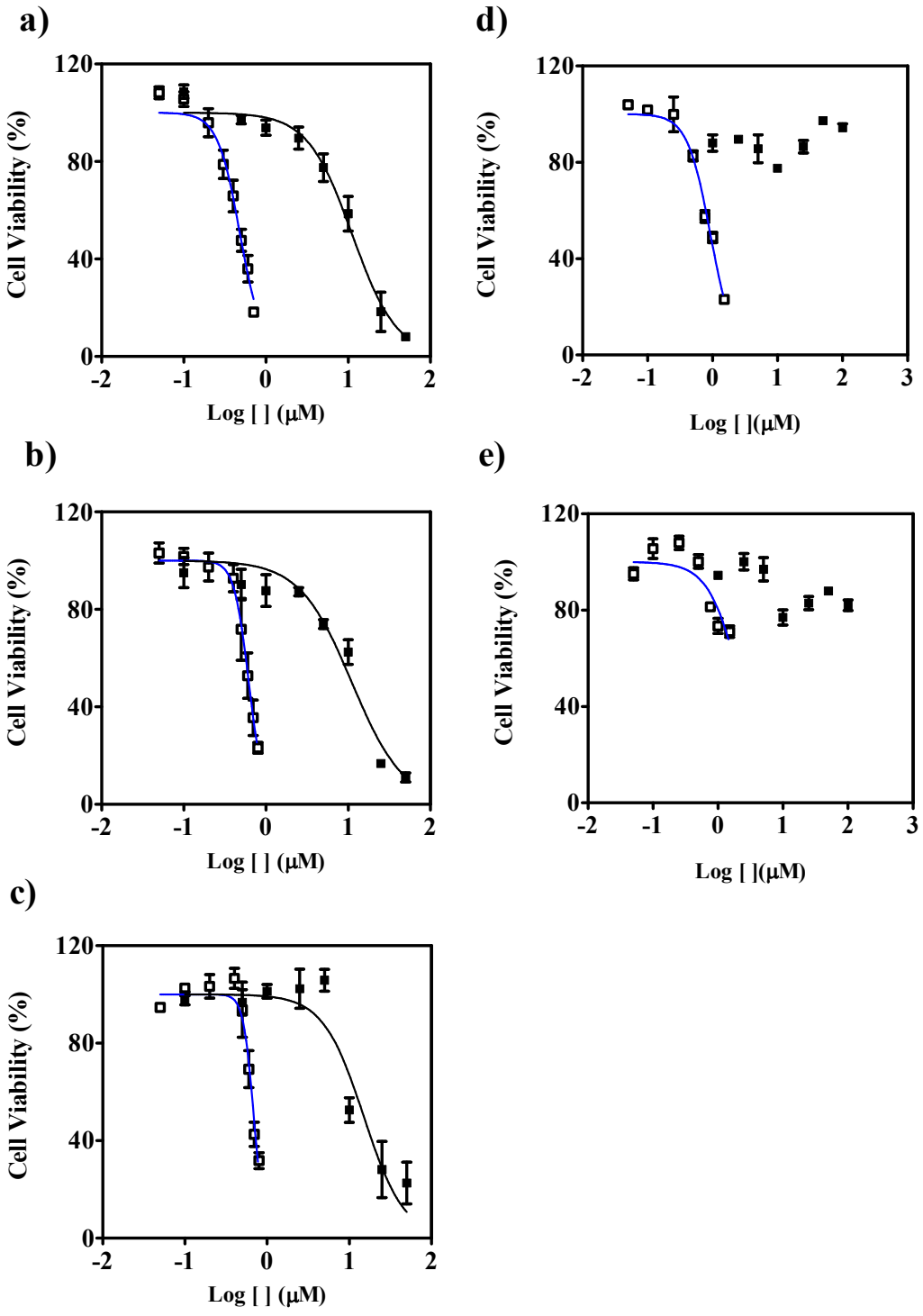

Figure S10. Dose-response curves for Pt MC and cisplatin treatments by the MTT assay. (A) HeLa (B) A2780 (C) A2790cis (D) HEK293 and (E) Human fibroblasts. Cells were incubated with three selected concentrations for 24 h. Data are the mean ± SD of three independent experiments. IC_{50} were calculated using non-linear regression using GraphPad Prism 5.0.

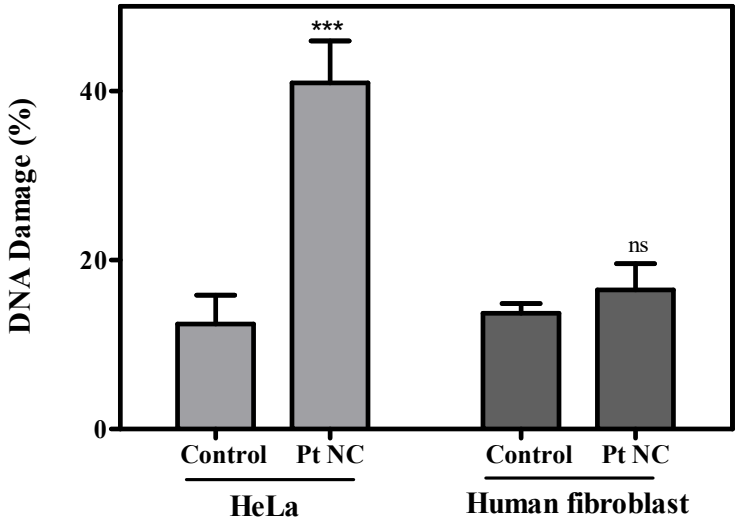

Figure S11. Quantitation of DNA damage of alkaline comet assay experiments by means of a 6-class visual classification score of HeLa and human fibroblast cells treated with Pt MC. Asterisks indicate significant differences between groups by the Student's t-test (***p < 0.01; ns: non-significant). Data are the mean of three independent experiments.

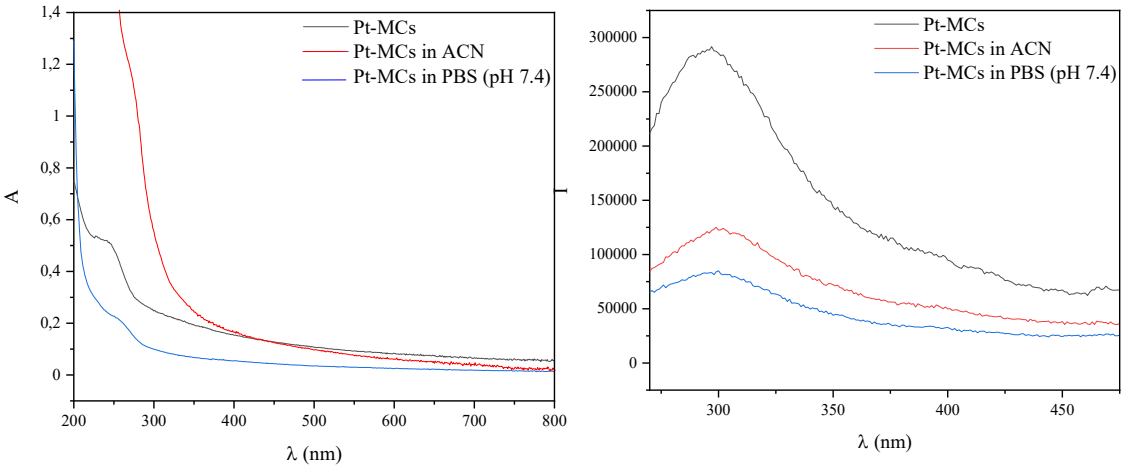

Figure S12. UV-vis absorption (left) and emission (fluorescence, right) spectra of Pt aqueous clusters under simulated intracellular conditions, mimicked with either acetonitrile solvent or PBS at pH= 7.4.

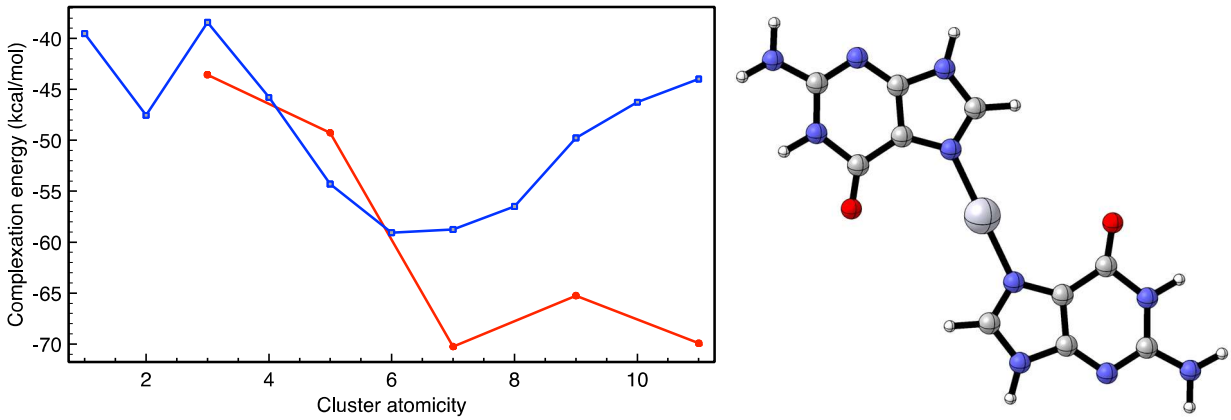

Figure S13. Graphical illustration of the complexation energy (in kcal/mol) as a function of the cluster atomicity (total number of atoms). Blue line stands for pure Pt metal clusters, while red line represents the energy of their oxidized counterparts. Right panel: Optimized structure for the model system associated to the attack of a single Pt atom to two guanine entities. According to DFT, the interaction energy is -82.04 kcal·mol^{-1}. This numeric value is consistent with the obtained result for the reaction of a Pt center with a single guanine (Pt–Guanine), which is -39.52 kcal·mol^{-1} (see Figure 4 in main text). Platination of two guanines by a Pt atom is therefore predicted with a double value.

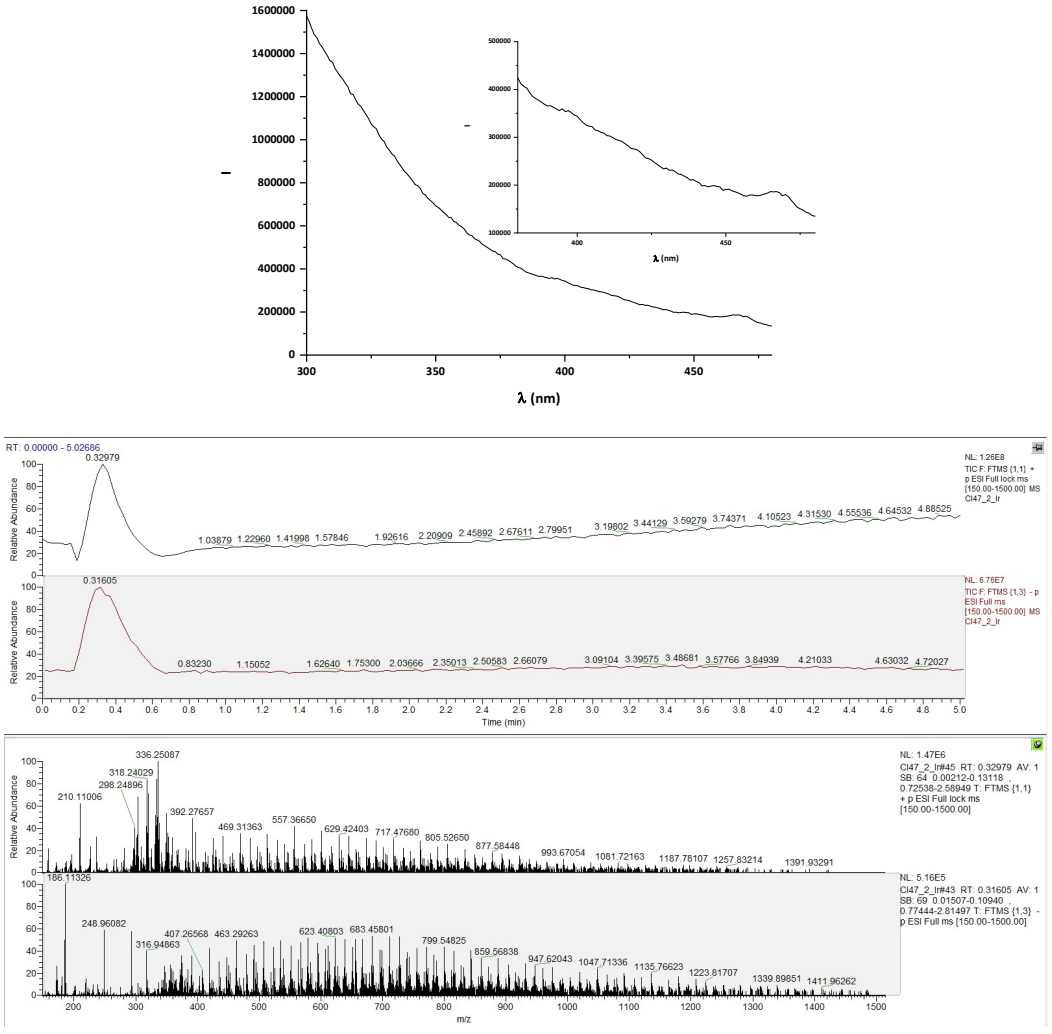

Figure S14. Emission (λ_{ex} = 280 nm) and Orbitrap measurements for Ir MCs.

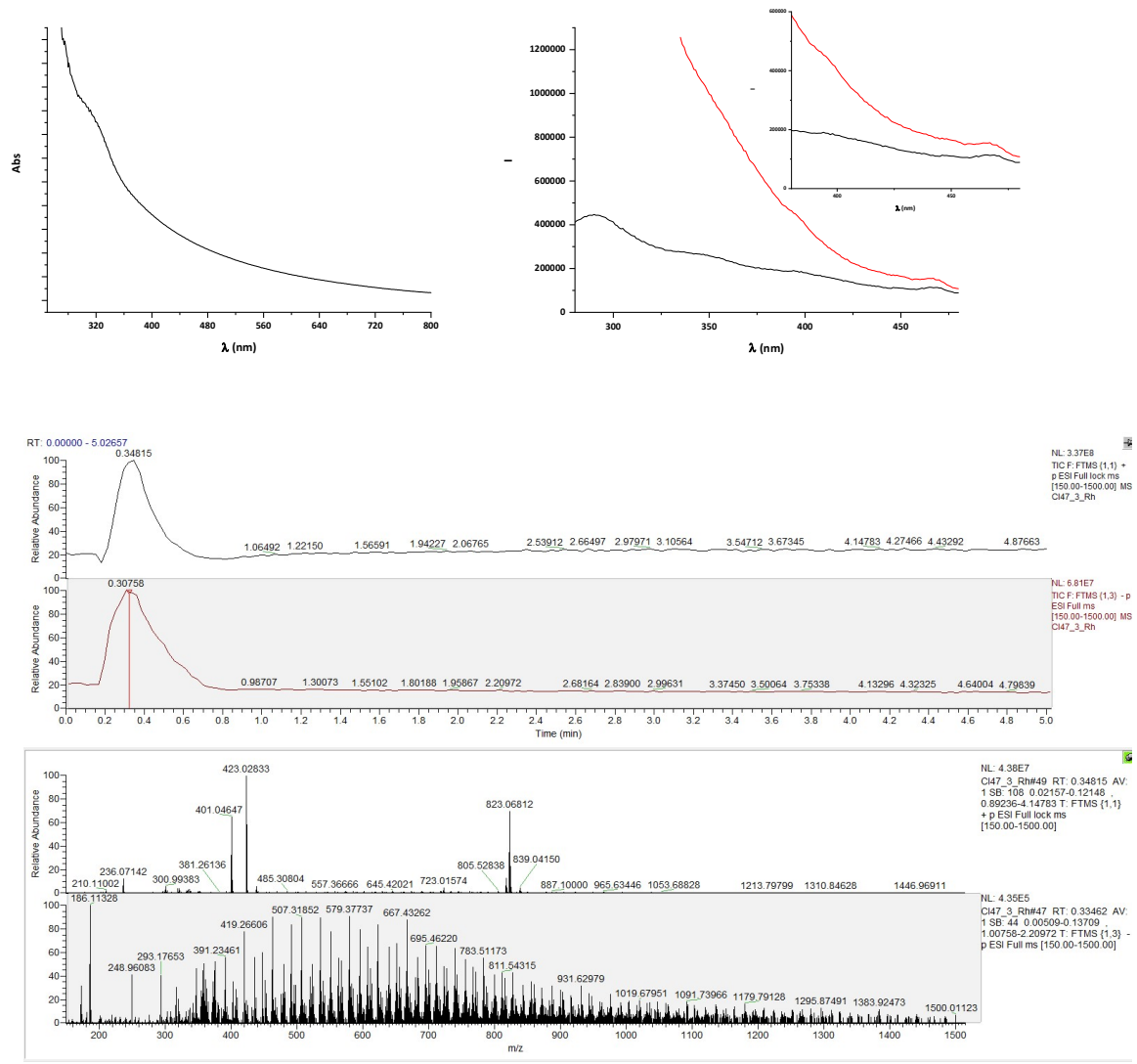

Figure S15. UV-vis adsorption, emission (λ_{ex} = 260 nm, 315 nm) and Orbitrap measurements for Rh MCs.

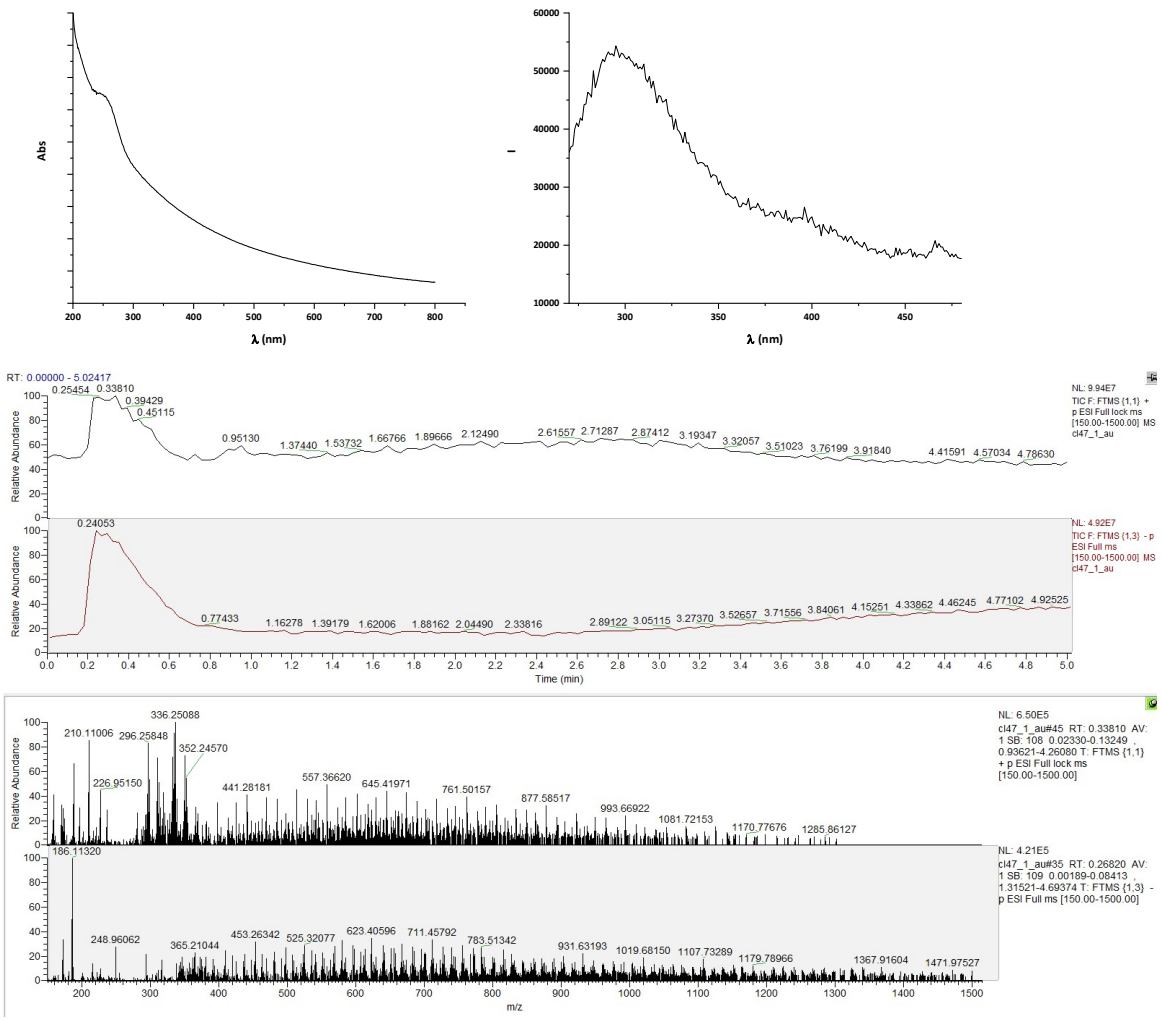

Figure S16. UV-vis adsorption, emission (λ_{ex} = 250 nm, 290 nm) and Orbitrap measurements for Au MCs.

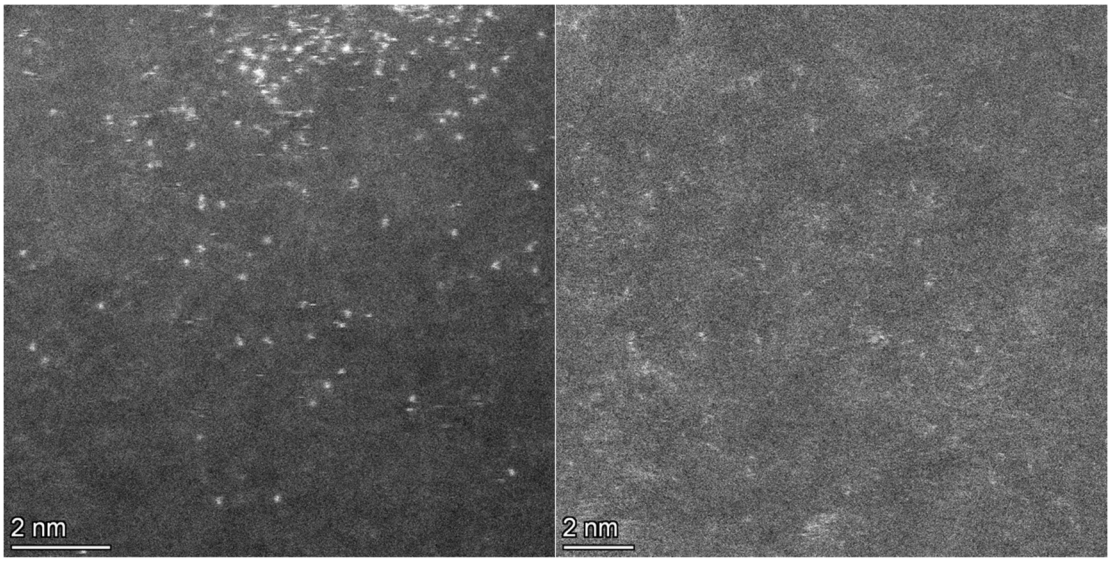

Figure S17. Visualization of Rh species on aqueous solution directly supported onto Cu-carbon grids, performed by means of High-Angle Annular Dark-Field HAADF- STEM images, which contrasts are related to the roughly Z^2 atomic number of the elements under the beam.

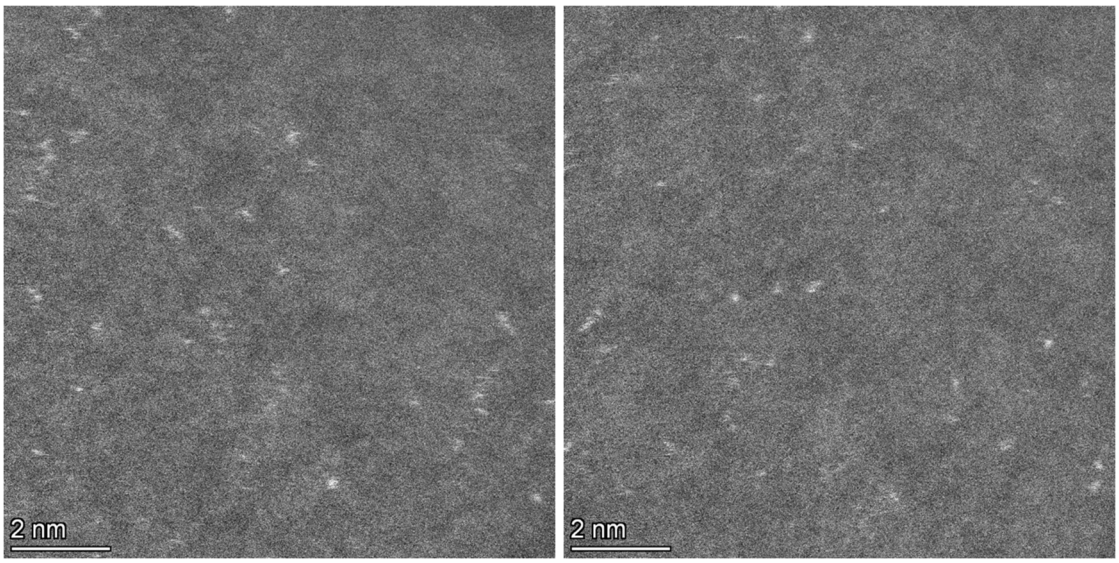

Figure S18. Visualization of Ir species on aqueous solution directly supported onto Cu-carbon grids, performed by means of High-Angle Annular Dark-Field HAADF-STEM images, which contrasts are related to the roughly Z^2 atomic number of the elements under the beam.

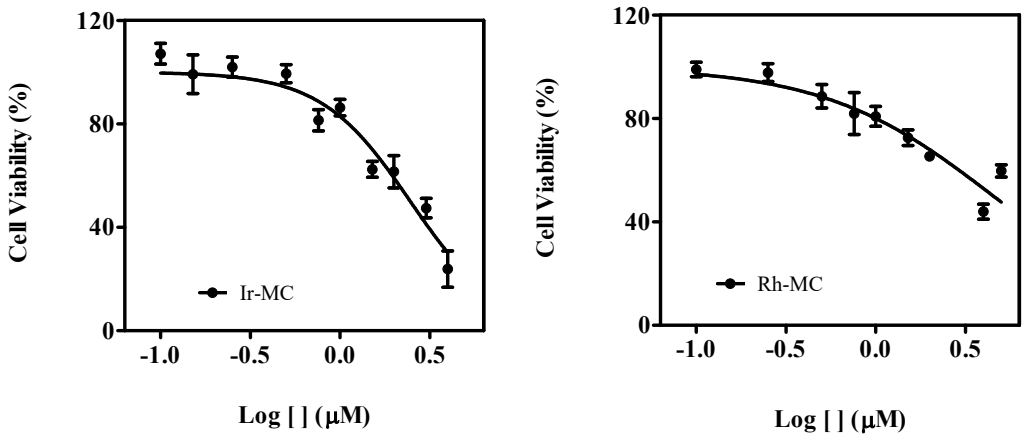

Figure S19. Effect of Ir-MC (left) and Rh-MC (right) on cell proliferation of HeLa cells analyzed by the MTT assay. Cells were incubated with concentrations ranging from 0.1 to 5 μM for 24 h. Data are the mean ± SD of three independent dose-response experiments.

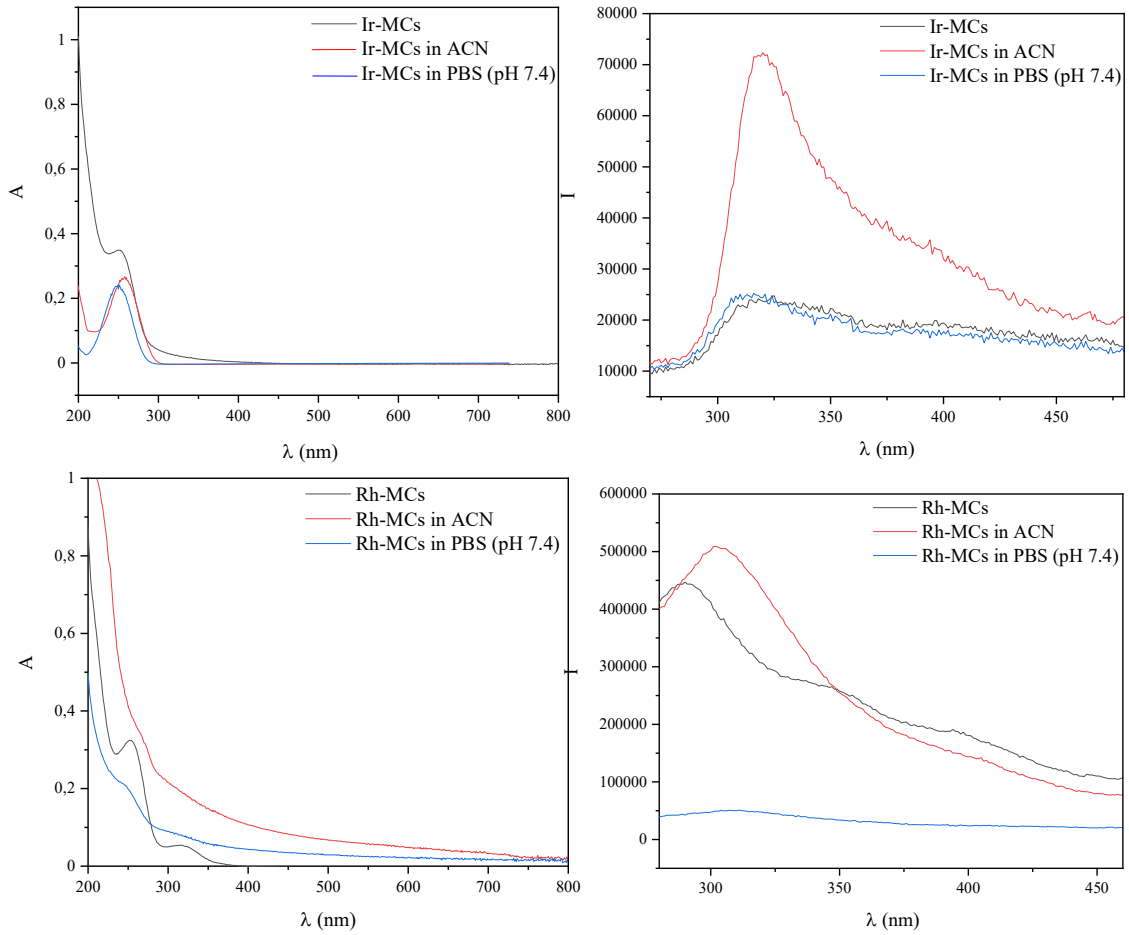

Figure S20. UV-vis absorption (left) and emission (fluorescence, right) spectra of Ir (top) and Rh (bottom) aqueous clusters under intracellular conditions, simulated with either acetonitrile solvent or PBS at pH= 7.4.

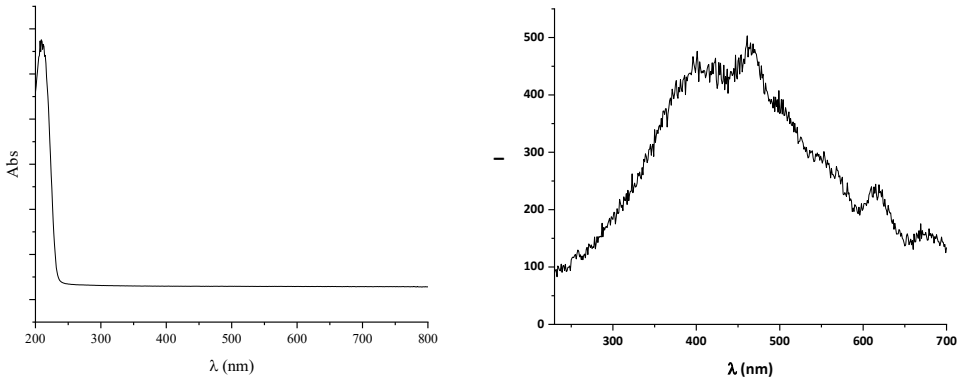

Figure S21. UV-Vis adsorption and emission of Pt clusters synthesized in PAMAM-G2.

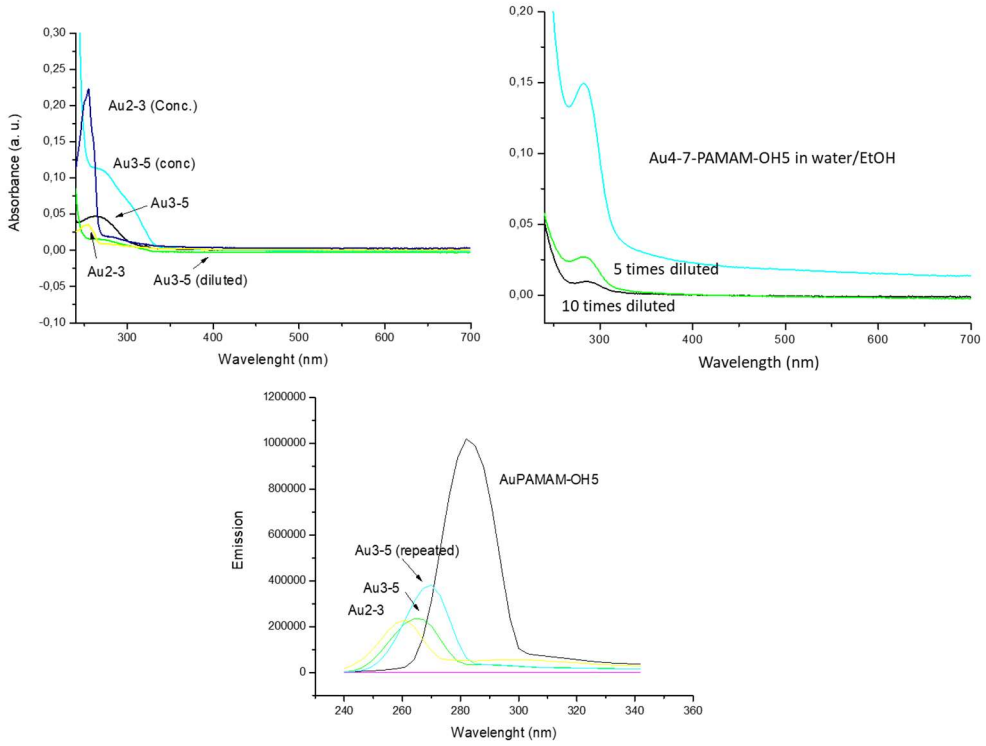

Figure S22. Absorption (top) and emission (bottom) UV/vis spectra for different mass-selected Au clusters prepared in water/EtOH mixtures by electrochemistry and provided by NANOGAP Co. and mass-selected Au clusters stabilized by PAMAM-OH5 (5^{th} generation in hydroxyl form) ligands in solution and selectively centrifugated.

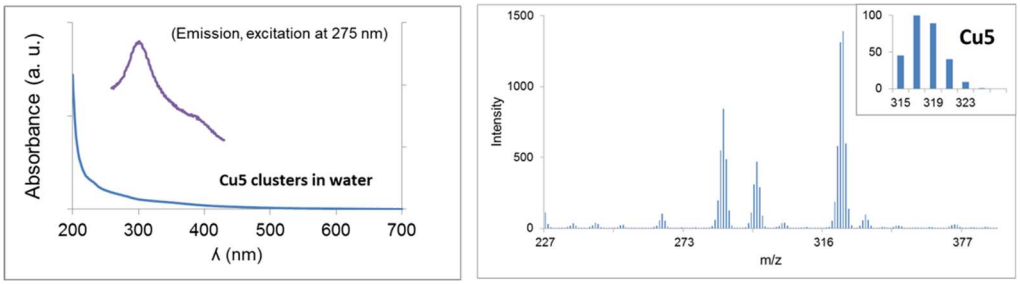

Figure S23. Left: Absorption and emission UV/vis spectra for Cu_5 clusters in water, synthesized by the electrochemical method and provided by NANOGAP Co. Right: Electrospray ionization-time of flight (ESI–TOF) mass chromatogram of Cu_5 clusters in ethanolic solution in negative ion mode. The inset shows the relative intensity peak simulation.

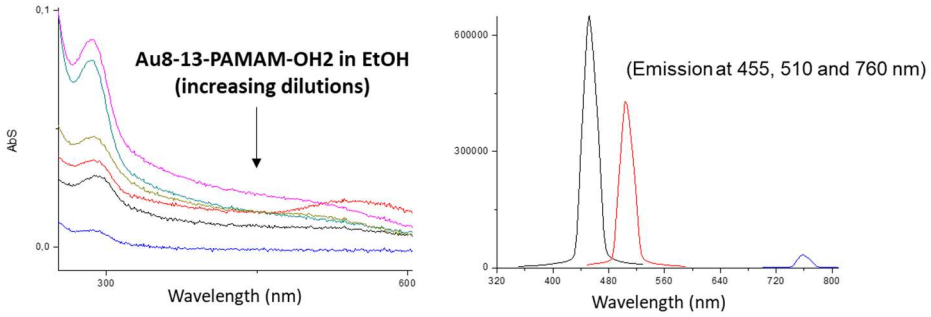

Figure S24. Absorption UV/vis spectra of and emission spectra for $Au_{8\text{-}13}$ atom clusters stabilized by PAMAM-OH2 (2^{th} generation in hydroxyl form) in EtOH, at increasing dilutions. A plasmonic band can be observed when the mixture was concentrated (red curve). Right: corresponding emision UV/vis spectra at different emission wavelength, which corresponds to Au_8 (60%), Au_{13} (30%) and Au_{21} (10%).

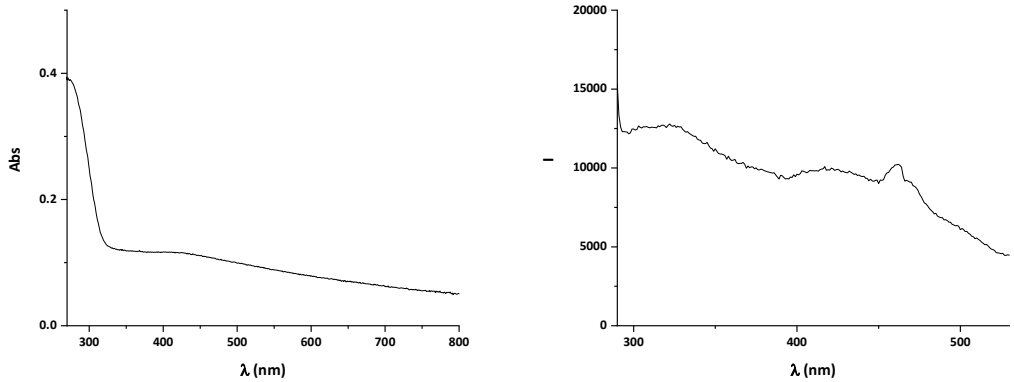

Figure S25. UV-Vis adsorption and emission of Au clusters synthesized in PAMAM-G2.

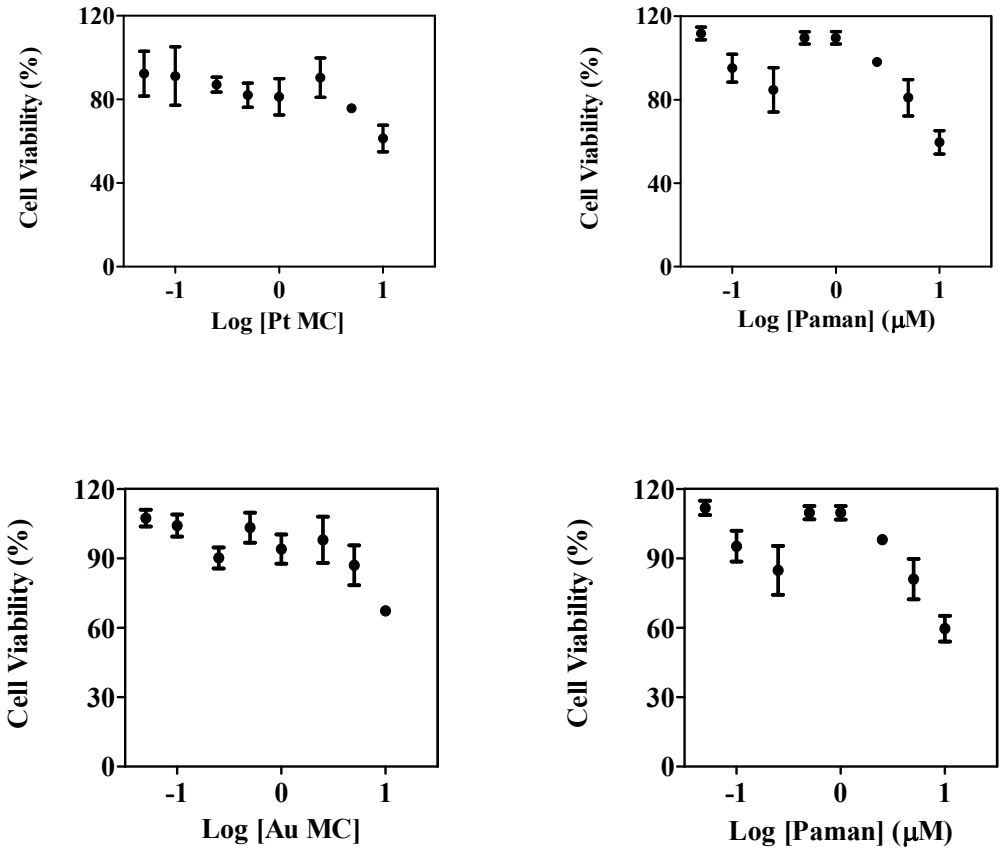

Figure S26. Cell proliferative analysis of HeLa cells with Pt_{5}-PAMAM-OH-5 (top) and $Au_{8\text{-}13}$ PAMAM-OH-2 (bottom), according to MTT assays. Au clusters of different atomicity and Cu clusters gave similar results, with the cell viability above PAMAM.

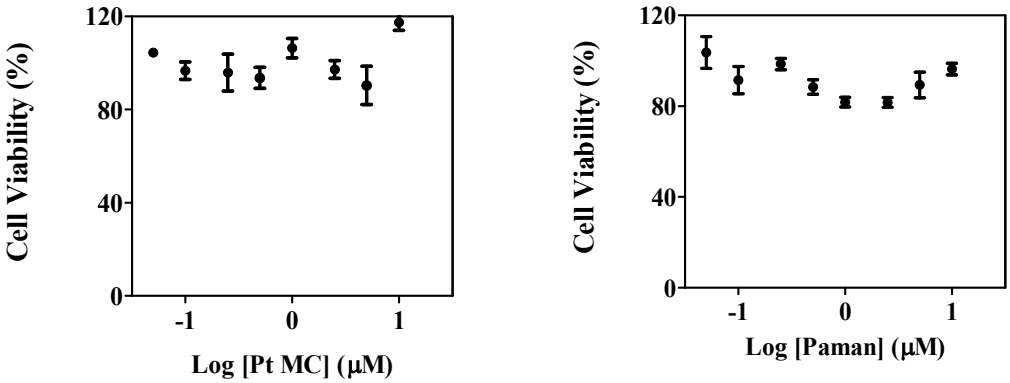

Figure S27. Dose-response viability curves of HeLacells with $Pt_{3\text{-}7}$-PAMAM-OH-5 (left) and pure PAMAM-OH5 (right), according to MTT assays.

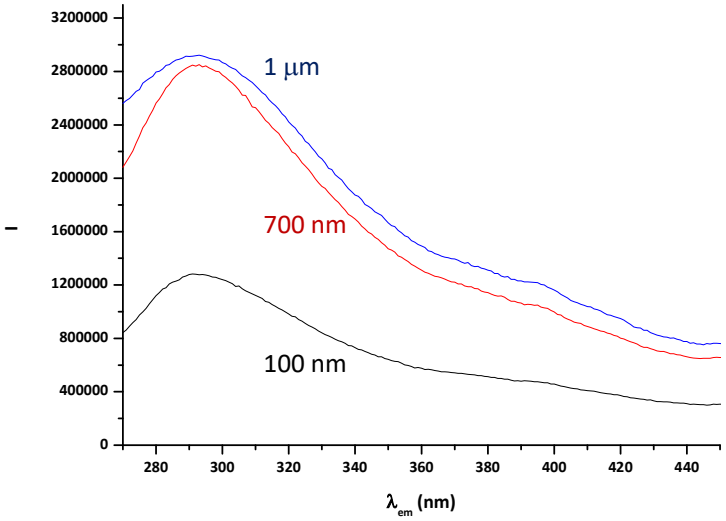

Figure S28. Left: Increasing fluorescence of independently synthesized 100 nM, 700 nM and 1 μM Pt clusters aqueous solution.

Supplementary Tables.

Table S1. Oxidation state calculation according to synchrotron measurements.

Sample	White Line	Oxidation State	Error estimation
Pt NPs	1.60559	0.97	0.136
Pt active clusters	1.52566	0.66	0.136
Pt inactive clusters	1.56608	0.82	0.136

References

S1 B. Ravel and M. Newville, *J. Synchrotron Rad.,* 2005, **12**, 537.

S2 O. Muller and R. Roy, *J. Less Common Met.,* 1968, **16**, 129.

S3 A. S. Chaves, M. J. Piotrowski and J. L. F. Da Silva, *Phys. Chem. Chem. Phys.,* 2017, **19**, 15484.

S4 C. Kerpal, D. J. Harding, A. C. Hermes, G. Meijer, S. R. Mackenzie and A. Fielicke, *J. Phys. Chem. A,* 2013, **117**, 1233.

S5 J. Reedijk, *Chem. Rev.,* 1999, **99**, 2499.

S6 J. V. Burda and J. Leszczynski, *Inorg. Chem.,* 2003, **42**, 7162.

S7 Y. Zhao and D. G. Truhlar, *Acc. Chem. Res.,* 2008, **41**, 157.

S8 F. Weigend and R. Ahlrichs, *Phys. Chem. Chem. Phys.,* 2005, **7**, 3297.

S9 H. P. Hratchian and H. B. Schlegel, in *Theory and Applications of Computational Chemistry: The First 40 Years* (Eds.: C. Dykstra, G. Frenking, K. Kim, G. Scuseria) Elsevier Science, Amsterdam, 2005.

S10 S. F. Boys and F. Bernardi, *Mol. Phys.,* 1970, **19**, 553.

S11 Gaussian 16, Revision B.01, Frisch, M. J.; Trucks, G. W.; Schlegel, H. B.; Scuseria, G. E.; Robb, M. A.; Cheeseman, J. R.; Scalmani, G.; Barone, V.; Petersson, G. A.; Nakatsuji, H.; Li, X.; Caricato, M.; Marenich, A. V.; Bloino, J.; Janesko, B. G.; Gomperts, R.; Mennucci, B.; Hratchian, H. P.; Ortiz, J. V.; Izmaylov, A. F.; Sonnenberg, J. L.; Williams–Young, D.; Ding, F.; Lipparini, F.; Egidi, F.; Goings, J.; Peng, B.; Petrone, A.; Henderson, T.; Ranasinghe, D.; Zakrzewski, V. G.; Gao, J.; Rega, N.; Zheng, G.; Liang, W.; Hada, M.; Ehara, M.; Toyota, K.; Fukuda, R.; Hasegawa, J.; Ishida, M.; Nakajima, T.; Honda, Y.; Kitao, O.; Nakai, H.; Vreven, T.; Throssell, K.; Montgomery, J. A., Jr.; Peralta, J. E.; Ogliaro, F.; Bearpark, M. J.; Heyd, J. J.; Brothers, E. N.; Kudin, K. N.; Staroverov, V. N.; Keith, T. A.; Kobayashi, R.; Normand, J.; Raghavachari, K.; Rendell, A. P.; Burant, J. C.; Iyengar, S. S.; Tomasi, J.; Cossi, M.; Millam, J. M.; Klene, M.; Adamo, C.; Cammi, R.; Ochterski, J. W.; Martin, R. L.; Morokuma, K.; Farkas, O.; Foresman, J. B.; Fox, D. J. Gaussian, Inc., Wallingford CT, 2016.